Real-time ultraviolet and column ozone from multichannel ultraviolet radiometers deployed in the National Science Foundation's ultraviolet monitoring network

Germar Bernhard
Charles R. Booth
James C. Ehramjian, MEMBER SPIE
Biospherical Instruments Inc.
5340 Riley Street
San Diego, California 92110
USA
E-mail: bernhard@biospherical.com

Abstract. Multichannel moderate-bandwidth ground-based ultraviolet (GUV) filter radiometers have recently been installed at several sites of the U.S. National Science Foundation's UV monitoring network where they complement high-resolution solar UV-100 (SUV-100) spectroradiometers. The five GUV channels are characterized for their spectral response and calibrated against SUV systems as well as irradiance standard lamps. Results indicate that accurate spectral characterization of GUV channels in the UV-B is crucial for obtaining high-quality UV measurements, in particular if instruments are calibrated with standard lamps. Using an inversion algorithm suggested by Dahlback (1996), total column ozone and approximately 30 different UV integrals and dose rates are routinely calculated from GUV measurements. For UV-A irradiance, GUV and SUV data agree to within ±5% for solar zenith angles (SZAs) up to 90 deg. A similarly good agreement can be achieved for the UV index if solar measurements are restricted to SZAs smaller than 78 deg. The agreement for data products that are dominated by wavelengths in the UV-B is generally worse, but can be substantially improved if GUV instruments are equipped with an additional channel at 313 nm. GUV total column ozone values agree on average to within ±5% with observations from the National Aeronautics and Space Administration's (NASA's) total ozone mapping spectrometer (TOMS) on board the earth probe satellite. GUV data products are disseminated via the website www.biospherical.com/NSF in near real time. [DOI: 10.1117/1.1887195]

Subject terms: solar ultraviolet radiation; multifilter radiometer; total column ozone; Antarctica; Arctic; quality assurance/quality contral.

Paper UV-12 received Apr. 9, 2004; revised manuscript received Aug. 30, 2004; accepted for publication Oct. 6, 2004; published online Apr. 6, 2005.

1 Introduction

The U.S. National Science Foundation's Office of Polar Programs (NSF/OPP) UV Monitoring Network was established in 1988 to collect UV data for interpreting the impact of ozone depletion. This network of six high-latitude sites, ranging from the South Pole, Antarctica, to Barrow, Alaska, acquires routine measurements of global (sun and sky) spectral irradiance between 280 and 600 nm at 1-nm resolution using solar UV-100 (SUV-100) spectroradiometers.[1,2] Preliminary data are disseminated weekly via the website www.biospherical.com/NSF and final data are published annually after extensive quality control procedures have been applied.

Moderate-bandwidth, multichannel ground-based UV (GUV) filter radiometers, designed and manufactured by Biospherical Instruments Inc., have recently been installed next to the SUV-100 spectroradiometers at several NSF/OPP network locations. The GUV instruments provide measurements at four approximately 10-nm-wide UV bands centered at 305, 320, 340, and 380 nm. A fifth channel either measures radiation at 313 nm (GUV-541) or photosynthetically active radiation (PAR) (GUV-511). The cosine error of the instruments is smaller than ±3% (±7.5%) for zenith angles less than 65 deg (82 deg). The instruments and their data have been described in several publications.[3–9]

GUV radiometers were added to the network for two reasons. First, GUVs have a simpler design than SUV-100s, and have no moving parts. This leads to enhanced short-term stability and makes GUVs a valuable tool for quality control of SUV-100 data. Second, UV data products such as the UV index or total column ozone can be calculated from GUV data in near real time and are made available via the Internet. These online data enable bridging the time between weekly updates from SUV-100 measurements, and may guide researchers at network sites in planning experiments.

Here we present and validate the method that is used by the NSF/OPP network to calculate UV data products and total ozone from GUV raw data. The conversion is based on a method suggested by Dahlback,[3] who has shown that erythemal (sun-burning) irradiance[10] (or the UV index[11]) can be derived from GUV instruments with good accuracy

0091-3286/2005/$22.00

Table 1 Specifications of the spectral characterization apparatus.

Monochromator	
Type	Czerny-Turner double monochromator in additive configuration with prism predisperser, designed and built by Biospherical Instruments Inc.
Focal length	500 mm
Focal ratio	*f*/5
Dispersion	0.35 nm/mm with 2400 g/mm gratings; 0.69 nm/mm with 1200 g/mm gratings
Bandwidth (FWHM)	1.35 nm with 2400 g/mm gratings; 2.6 nm with 1200 g/mm gratings
Wavelength accuracy	$\pm$0.1 nm
Light source	1000-W xenon arc lamp from Oriel Instruments
Reference detector	Silicon photodiode, Newport Corporation, Model 818-UV, responsivity calibration traceable to the National Institute of Standards and Technology (NIST)

using this method. An additional objective of this paper is to extend Dahlback's method to UV effects other than erythema.

GUV measurements presented in this publication were calibrated and compared with SUV-100 and SUV-150B spectroradiometers. The SUV-150B spectroradiometer is an advanced version of a SUV-150 spectroradiometer described previously.[2,12] Compared to its predecessor and the SUV-100, the SUV-150B features an upgraded wavelength drive with optical encoders, which reduce wavelength uncertainties to $\pm$0.015 nm. The collector's cosine error is smaller than $\pm$2% for zenith angles smaller than 75 deg. The instrument has participated in the 2003 North American UV Intercomparsion, held at Boulder, Colorado, between June 16 and 22, 2003 (manuscript is in preparation). Preliminary data analysis indicates that the instrument agreed with other participating instruments to within a few percent.

2 Spectral Response Characterization

To obtain the most accurate results from GUV data, it is best to characterize each instrument individually to account for small variations in the transmission characteristics of their interference filters. For example, variations of several tenths of 1 nm in the center wavelength of the filters are within the tolerance specifications of the filter manufacturer. Until recently, only data from subcomponents (i.e., diffusers, filters, detectors) could be used to calculate the spectral response functions of GUV channels. To overcome this limitation, we developed an apparatus for characterizing the spectral response of assembled GUVs directly.

The apparatus consists of a 1000-W xenon arc lamp from Oriel Instruments and a grating double monochromator with prism predisperser, designed and built by Biospherical Instruments Inc. The two single monochromators that make up the double monochromator are stacked vertically and share a common shaft to which the gratings are mounted. This design ensures that the two single monochromators are always synchronized. Gratings with 2400 grooves per mm (g/mm) are used for characterizing GUV channels in the UV. Gratings with 1200 g/mm are utilized for measuring the PAR channel.

The intensity of radiation exiting the monochromator is characterized as a function of the monochromator's wavelength setting with a calibrated silicon photodiode. For determining the wavelength mapping of the monochromator, a mercury discharge lamp is used. Table 1 gives an overview of the specifications of the apparatus.

The spectral response of a GUV channel is determined by comparing the GUV output signal against the signal of the reference silicon photodiode as a function of wavelength in 1-nm steps. Data reduction includes the following steps: (1) wavelength correction of spectra measured with the silicon photodiode and each of the GUV channels, (2) subtraction of dark currents from the signals measured by the silicon photodiode and the GUV channels, (3) radiometric calibration of the net-signals of all GUV channels based on the spectrum measured with the silicon photodiode, (4) deconvolution of the calibrated GUV signals to reduce the ''smoothing'' effect of the monochromator's finite resolution, and (5) normalization of the deconvolved result. The deconvolution algorithm of step (4) is based on the following approximation:

$$\frac{R_D(\lambda)}{R_M(\lambda)} \approx \frac{R_M(\lambda)}{R_C(\lambda)}, \tag{1}$$

where

$R_D(\lambda)$=deconvolved spectral response (which ideally is the true spectral response)

$R_M(\lambda)$=measured spectral response after step (3) normalized to 1 at the maximum value

$R_C(\lambda)$=measured spectral response convolved with the slit function of the monochromator

Given $R_M(\lambda)$, $R_C(\lambda)$ can readily be calculated, and $R_D(\lambda)$ can be estimated by rearranging Eq. (1). The resulting deconvolved spectral response is somewhat affected by noise in the measurement. To reduce this effect, $R_M(\lambda)$ is set to 0.0001 if the normalized response is smaller than 0.0001. The deconvolved result is limited to four orders of magnitude due to this restriction.

Figure 1 illustrates the deconvolution technique with measurements of the 320-nm channel of GUV S/N 29236.

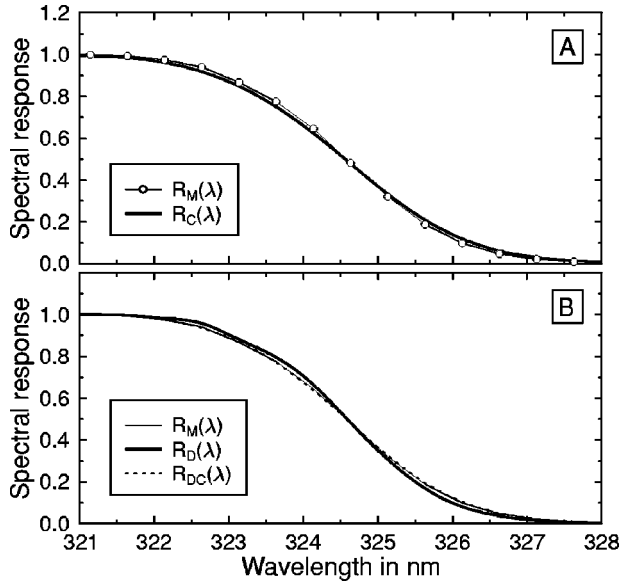

Fig. 1 Spectral response functions of the long-wavelength side of the 320-nm channel from GUV S/N 29236: (a) comparison of measured response $R_M(\lambda)$ with convolved response $R_C(\lambda)$ and (b) comparison of measured response $R_M(\lambda)$ with deconvolved response $R_D(\lambda)$ and with response $R_{DC}(\lambda)$, which was calculated by convolving $R_D(\lambda)$ with the slit function of the test apparatus.

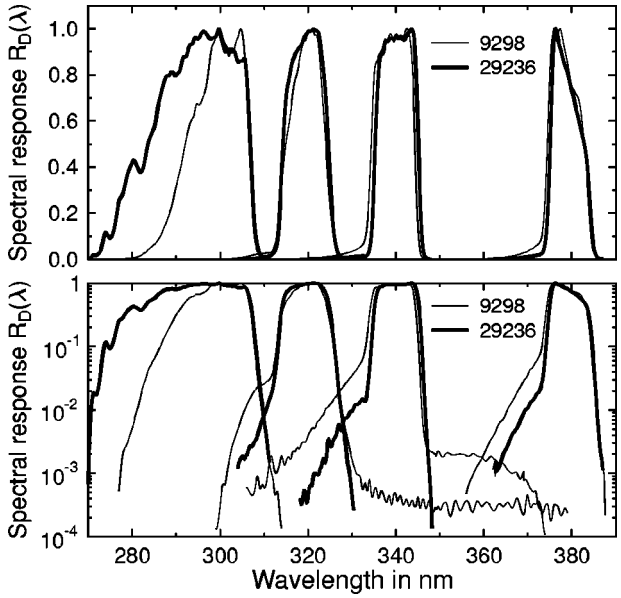

Fig. 2 Spectral response functions $R_D(\lambda)$ of the 305-, 320-, 340-, and 380-nm channels of two GUV radiometers (S/N 9298 and 29236) in linear (upper panel) and semilogarithmic (lower panel) presentation.

The figure indicates that the deconvolved spectral response $R_D(\lambda)$ has a steeper cutoff than the original measurement $R_M(\lambda)$. The quality of the deconvolution technique was checked by convolving $R_D(\lambda)$ with the slit function of the monochromator and comparing the resulting function, denoted $R_{DC}(\lambda)$, with the original measurement $R_M(\lambda)$. If the deconvolution were perfect, $R_{DC}(\lambda)$ and $R_M(\lambda)$ would be equal. For the example shown in Fig. 1, $R_{DC}(\lambda)$ and $R_M(\lambda)$ are barely distinguishable [i.e., the difference of $R_M(\lambda)$ and $R_{DC}(\lambda)$ is less than 0.01], suggesting that the accuracy of measurements with the test apparatus is improved by this simple approach.

Figure 2 shows the spectral response functions $R_D(\lambda)$ of the 305-, 320-, 340-, and 380-nm channels for two GUV radiometers (S/N 9298 built in 1996 and S/N 29236 built in 2001). There are several points that are worth noting:

1. The short-wavelength limits of the 305 channel of both radiometers are shifted by approximately 8 nm due to the different set of filters and detectors used in the instruments. This difference has very little impact on measurements of sunlight, as solar radiation below 290 nm does not penetrate the earth's atmosphere. Almost all contributions to the 305-nm GUV signal results from photons with wavelengths between 300 and 310 nm, where the response functions of the two instruments are very similar.
2. The detector of the 305-nm channel is a phototube with no significant sensitivity above 315 nm. Photons with wavelengths in the UV-A or visible, which may reach the surface of the detector due to possible light leaks of the filters, are not detected.
3. The responsivities of the 320-, 340-, and 380-nm channels are similar for both instruments, but are shifted by 0.6 to 0.9 nm relative to one another. These shifts are caused by the different transmission characteristics of the interference filters used in the two instruments.
4. The lower panel of Fig. 2 indicates that the 320-nm channel of GUV S/N 9298 is also sensitive to radiation in the 330- to 380-nm band. Likewise, the 340-nm channel is also sensitive between 350 and 370 nm. Such light leaks can introduce significant errors in solar measurements, particularly when the detector is also sensitive to radiation in the visible. We quantified the effect of light leaks of the two channels by weighting model spectra with the original response functions and with modified functions that excluded the light leak portion. Model spectra were calculated for solar zenith angles (SZAs) between 0 and 90 deg and total ozone values between 100 and 600 Dobson units (DU). The difference between the two data sets was less than 1% for SZA$<$80 deg, indicating that the leakage problem is too small to affect solar data appreciably.

3 Calibration

The calibration factors k_i for each GUV channel i were determined with a method originally proposed by Dahlback[3]:

$$k_i = \frac{V_i - O_i}{\int_0^\infty R_{D_i}(\lambda) E(\lambda) \mathrm{d}\lambda} = \frac{V_i - O_i}{W_i}, \tag{2}$$

where $E(\lambda)$=spectral irradiance at the plane of the GUV's collector

V_i=the signal of channel i

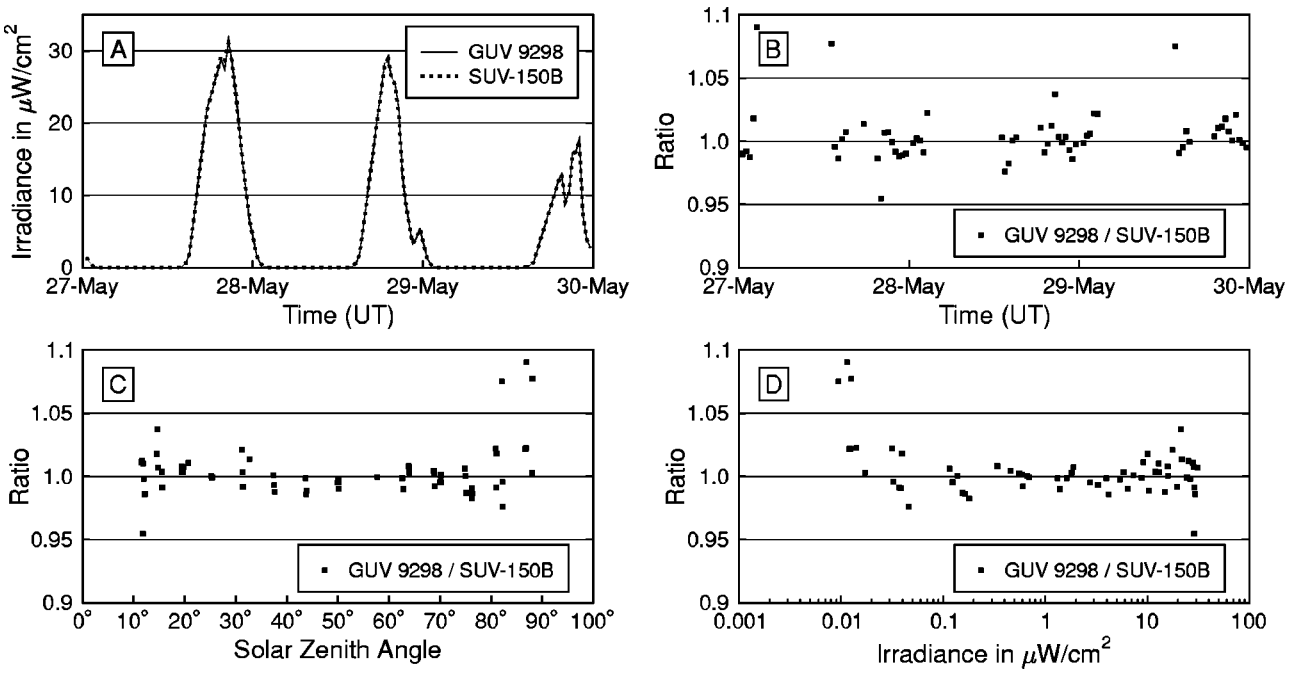

Fig. 3 Comparison of measurements from the 305-nm channel of GUV S/N 9298 and the SUV-150B: (a) irradiance measured by GUV and SUV as a function of time, (b) ratio GUV/SUV as a function of time, (c) ratio GUV/SUV as a function of SZA, and (d) ratio GUV/SUV as a function of spectral irradiance (note the logarithmic *x* axis).

O_i=offset of channel *i*, inferred from measurements at night or by covering the collector

$R_{D_i}(\lambda)$=deconvolved, normalized spectral response of channel *i*

W_i=spectral irradiance weighted with the spectral response of channel *i*

The values of k_i are independent of the light source that produces $E(\lambda)$ if $R_{D_i}(\lambda)$ represents the true spectral response functions of the radiometer channels. In this paper, the sources for $E(\lambda)$ are either the sun or standard lamps, which have calibrations traceable to the National Institute of Standards and Technology (NIST). In the case of sunlight, spectral irradiance was measured using SUV-100 or SUV-150B spectroradiometers, which were installed adjacent to the GUV under test.

Figure 3 shows a comparison of solar measurements from the 305-nm channels of GUV S/N 9298 and a SUV-150B. Prior to this comparison, the calibration factor k_{305} of the GUV was calculated by regressing the net-signal of the GUV [numerator of Eq. (2)] against W_{305}. Accurate synchronization of both instruments is crucial for this correlation. The GUV minute-by-minute measurements were interpolated to match the time when the SUV-150B was scanning at 305 nm. Owing to the way k_{305} is established, a good agreement of GUV and SUV data at small SZAs can be expected. Figure 3 demonstrates that a high level of agreement is also achieved at SZAs as large as 85 deg. With the exception of three points, the ratio of GUV and SUV-150B measurements agree to within ±5%. The three outliers occur at SZAs larger than 82 deg when irradiance levels are more than three orders of magnitude below the noon-time maximum [Fig. 3(d)].

Good agreement between the GUV and SUV-150B data could be achieved only because the spectral response functions of the GUV channels were accurately known. To demonstrate this, we deliberately shifted the measured response functions of GUV S/N 9298 by 0.5 nm, and repeated the analysis presented in Fig. 3. A comparison of the shifted and unshifted data sets is presented in Fig. 4. The effect of the shift is most pronounced for the 305-nm channel due to the rapid change of the solar spectrum in this wavelength range [Fig. 4(a)]. At small SZAs, the ratio GUV/SUV is close to unity also for the shifted data set due to the way the calibration is established. At SZA=75 deg, both data sets disagree by 14%. The disagreement is caused by the fact that the shape of the solar spectrum changes as a function of SZA over the wavelength interval where the GUV 305-nm channel is sensitive. The relative change of the spectral distribution of solar radiation is sufficiently different for the shifted and unshifted wavelength intervals to explain the SZA-dependence indicated in Fig. 4(a). The change of the solar spectrum with SZA is much smaller at 320 nm, resulting in a smaller (but still significant) difference of the shifted and unshifted datasets [Fig. 4(b)].

A further validation of the accuracy of the calibration factors k_i can be obtained by evaluating the results of solar- and lamp-based calibrations. Figure 5 presents a comparison of calibration factors established with the two methods for three different GUVs (S/Ns 29235, 29236, and 9298). The spectral response functions of all instruments have been measured as described in Sec. 2. Calibration factors for GUV S/N 9298 that were calculated with the set of shifted response functions discussed above were also compared.

Figure 5 shows that solar- and lamp-based calibration

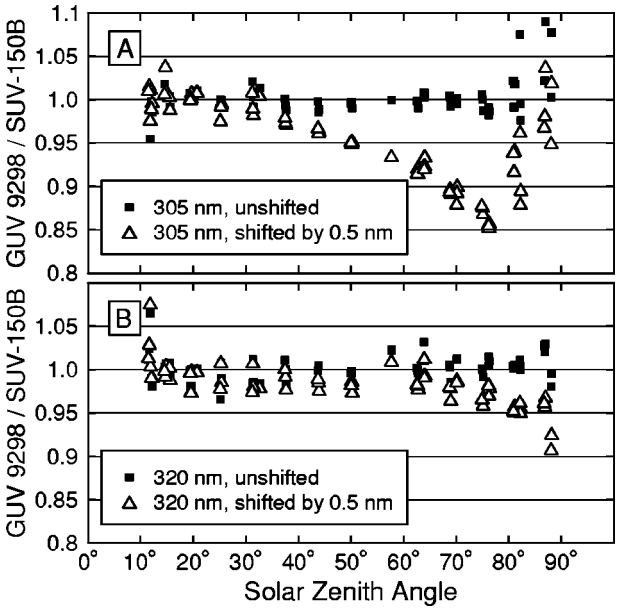

Fig. 4 Comparison of measurements from the 305- and 320-nm channels of GUV S/N 9298 and the SUV-150B using either the measured, unshifted GUV response functions $R_{D_i}(\lambda)$ (solid squares) or response functions constructed by shifting $R_{D_i}(\lambda)$ by 0.5 nm (open triangles) for (a) the GUV 305-nm channel [the unshifted data set is identical with the one shown in Fig. 3(c)] and (b) the GUV 320-nm channel.

factors agree to within ±3% if the measured response functions are used. This is a good result as differences of 3% are well within the measurement uncertainties of the SUV-150B and lamp-based GUV calibrations. In contrast, if the shifted response function for the 305-nm channel of GUV S/N 9298 is used, solar- and lamp-based calibration factors deviate by 14%. By comparing the difference in the factors for the shifted and unshifted results, we determined that solar data from the 305-nm channel will be incorrect by 12% if the calibration factor of this channel is established from a lamp measurement, and the response function used for the calculation has a wavelength error of 0.5 nm.

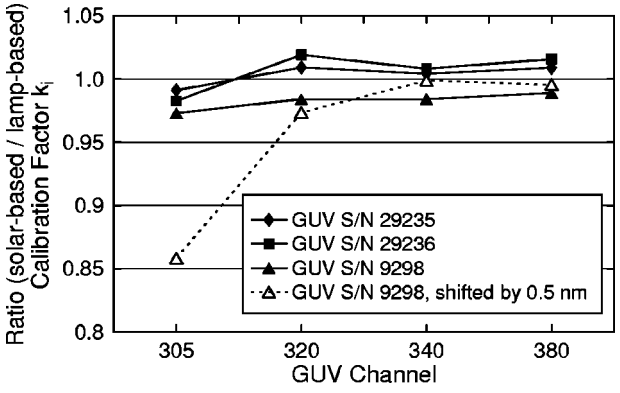

Fig. 5 Comparison of solar- and lamp-based calibration factors k_i for three different GUV radiometers. The calibration factors marked with solid symbols were calculated with the measured response functions of the radiometers. The data set marked with open triangles was calculated with the shifted response functions of GUV S/N 9298 (shift=0.5 nm) to investigate the effect of wavelength errors on the resulting calibration factors.

Figure 5 also indicates that wavelength shifts have a much smaller effect for the 320-, 340-, and 380-nm channels. For example, the effect of a shift of 0.5 nm on the 320-nm channel is only 1.1%. This suggests that accurate solar measurements can be expected from lamp-based calibrations for all but the 305-nm channel, even if the response functions used for the calibration are not ideally defined.

4 Data Products

4.1 *UV Dose Rates and Integrals*

The conversion from response-function-weighted irradiance W_i to useful data products D, such as erythemal irradiance, is performed with the method suggested by Dahlback.[3] In brief, D is approximated by a linear combination of the net voltages from the GUV channels:

$$D=\sum_i a_i(V_i-O_i). \tag{3}$$

The coefficients a_i are calculated by solving the system of linear equations [see also Eq. (7) of Dahlback[3]]:

$$\sum_i \left[a_i k_i \int_0^\infty R_{D_i}(\lambda) E_{M_j}(\lambda) \mathrm{d}\lambda \right] = \int_0^\infty A(\lambda) E_{M_j}(\lambda) \mathrm{d}\lambda, \tag{4}$$

where $A(\lambda)$ is the action spectrum of the biological effect under consideration, and $E_{M_j}(\lambda)$ are model spectra calculated for different SZAs and ozone columns. These spectra are required to quantify the relative spectral difference between the response functions and the action spectrum. For this paper, model spectra were calculated with the radiative transfer model UVSPEC/libRadtran.[13] The number of GUV channels i may range between 1 and 5, depending on the action spectrum used, and the number of model spectra required for the inversion has to match this number. For example, to calculate the set of coefficients a_i for the erythema action spectrum for a GUV deployed at San Diego, we used all four GUV-511 UV channels, and four model spectra calculated for combinations of SZA and total ozone of 30 deg, 250 DU; 30 deg, 400 DU; 70 deg, 250 DU; and 70 deg, 400 DU. The values of the coefficients a_i determined with this method are not very sensitive to the choice of model parameters. We quantified this sensitivity by calculating erythemal dose rates from GUV measurements at San Diego with different sets of model spectra. When the inversion was based on a set of spectra calculated for an elevation of 1700 rather than 0 m, erythemal dose rates changed by less than ±1% ($\pm 1\sigma$) for SZAs smaller than 80 deg. Changing surface albedo from 3 to 80% in the model modified dose rates by less than ±1% ($\pm 1\sigma$) for SZAs smaller than 70 deg and led to approximately 2% higher dose rates at SZA=80 deg. Changing the wavelength dependence of aerosol extinction within reasonable limits altered dose rates by less than 0.1%. Larger differences for other data products cannot be excluded and are discussed below. To obtain the most accurate results, model input parameters were chosen to match the prevailing con-

Table 2 GUV data products.

Spectral irradiance[a]		
305, 320, 340, 380, 400, 500, and 600 nm		
Integrals[b]		
290 to 315, 290 to 320, 315 to 360, 320 to 360, 360 to 400, 315 to 400, 320 to 400, and 400 to 600 nm		
Dose rates		
Effect	References	Remarks
Erythema	CIE,[10] Komhyr and Machta,[14] Diffey,[15] Anders et al.[16]	Four different action spectra are implemented.
UV Index	CIE[10,11]	
DNA damage	Setlow[17]	Four parameterizations of the action spectrum are implemented.
Skin cancer in mice	Gruijl et al.[18]	Often referred to as SCUP-m
Skin cancer in mice corrected for human skin	Gruijl et al.[18]	Often referred to as SCUP-h
Generalized plant damage	Caldwell[19]	
Plant growth	Flint and Caldwell[20]	
Damage to anchovy	Hunter et al.[21]	
Inhibition of phytoplankton carbon fixation	Boucher and Prezelin[22]	
Inhibition of phytoplankton photosynthesis of phaeodactylum and prorocentrum	Cullen et al.[23]	
Inhibition of photosynthesis in Antarctic phytoplankton	Neale and Kieber[24]	
Additional		
Spectral irradiance weighted with the response of several broadband filter radiometers, PAR, total column ozone		

[a]The "action spectra" $A(\lambda)$ for the calculation of spectral irradiances are triangular functions with a bandwidth of 1 nm FWHM centered at the specified wavelengths.

[b]The "action spectra" $A(\lambda)$ for the calculation of integrals are rectangular functions set to 1 within the specified intervals and to 0 outside these intervals.

ditions at the deployment sites of GUVs. Note that the method just outlined required further assumptions on atmospheric composition and radiative transfer that may not always describe the actual situation well. Additional systematic errors may, for example, exist at highly polluted locations. It can therefore be expected that data products derived from filter instruments have larger uncertainties than data products calculated directly from high-resolution spectroradiometric measurements.

As an alternative to the outlined inversion method, the coefficients a_i could also be determined by multiple linear regression of the GUV net voltage against biologically weighted spectra from spectroradiometers.[4] The inversion method has some advantages compared to this alternative method:

1. If the response functions $R_{D_i}(\lambda)$ are accurately known, the coefficients a_i can be calculated from lamp-based calibration factors k_i. It is therefore not required to operate a GUV side-by-side with a high-resolution spectroradiometer for several days, as in the case of the alternative method.
2. The prevailing conditions at the location where the calibration is established may be different from the conditions at the deployment site, which may bias the regression results. For example, if a GUV is calibrated with the alternative method in San Diego and deployed in Antarctica, prevailing SZA, total ozone, and albedo will be very different.

We are currently calculating 15 different wavelength integrals and 15 different dose rates from GUV data with the method outlined above. Table 2 gives an overview of the wavelength bands and action spectra implemented.

To validate the conversion introduced method, we compared integrals and dose rates measured by GUV and SUV-100 radiometers at San Diego, the South Pole, McMurdo, and Palmer Station. The SUV-150B spectroradiometer data set contains only a limited time series and is not presented here. Calibration factors k_i were calculated by regressing GUV net signals against weighted irradiances from collocated SUV-100 spectroradiometers, as described in Sec. 3. Linking the GUV calibrations to collocated SUV-100 system should ideally result in identical data products from the two instruments. However, possible systematic errors in SUV-100 measurements will also affect the absolute accuracy of GUV data. For example, SUV-100 data used here were not corrected for the instrument's cosine errors and are therefore 5 to 10% low, depending on SZA and data product. A cosine-corrected SUV-100 data set has recently become available for South Pole.[25] We also calibrated GUV

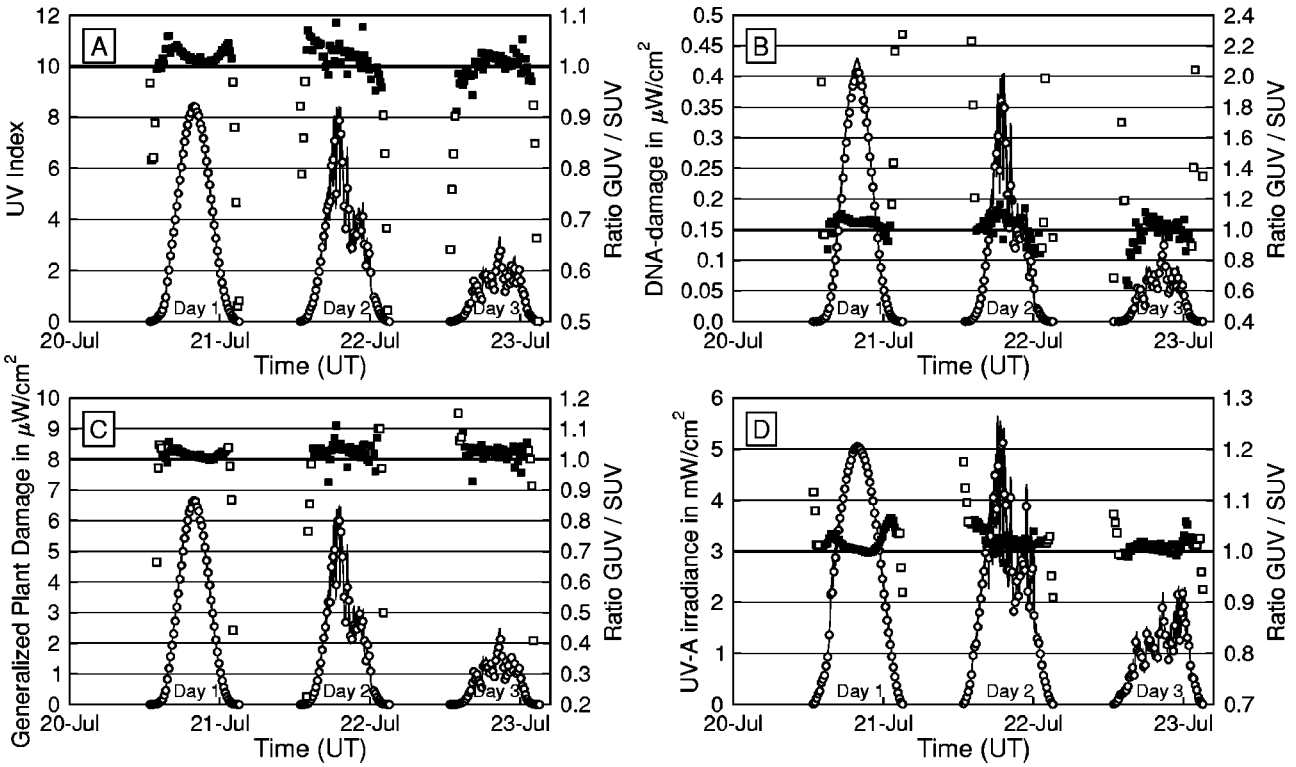

Fig. 6 Comparison of four different data products measured by GUV S/N 9298 (line, left axis) and SUV-100 (open circles, left axis) at San Diego between July 20 and July 24, 2003. GUV data are 1-min averages, SUV data were calculated from spectra measured every 15 min for (a) UV index, (b) DNA-damaging radiation, (c) generalized plant damage, and (d) UV-A (320 to 400 nm). For (a) and (d), solid (open) squares indicate the ratios of GUV and SUV measurements for SZA$<$80 deg ($>$80 deg). For (b) and (c), solid (open) squares indicate the ratio GUV/SUV for SZA$<$70 deg ($>$70 deg).

measurements against this data set and include results in the following presentation.

The GUVs at Palmer Station and McMurdo (S/Ns 29230 and 29234) were deployed before the apparatus for measuring spectral response function was available. In absence of actual response data for the two instruments, we implemented the measured response functions of GUV S/N 29239. For the 320-, 340-, and 380-nm channels, the functions of GUV S/N 29239 were used without modification. For the 305-nm channels, the response function of GUV S/N 29239 was shifted until the SZA dependence of the ratio of calibrated GUV data and weighted SUV-100 spectra became minimal. The shift was determined to be 0.9 nm for GUV S/N 29234 and 0.0 nm for GUV S/N 29230. This approach is not ideal, but led to acceptable results.

Figure 6 shows a comparison of GUV and SUV-100 results for four data products: the UV index,[11] DNA-damaging radiation,[17] generalized plant damage,[19] and UV-A. The data were measured at San Diego between July 20 and July 24, 2003. Day 1 was cloudless, day 2 had variable cloud cover, and day 3 was overcast (see Fig. 6 for day assignment). The UV-index and UV-A measurements of the two instruments agreed to within $\pm 10\%$ (maximum deviation) for all three days when SZAs were smaller than 80 deg. The agreement for the DNA- and plant-damage data sets are similar when the data sets are filtered for SZAs smaller than 70 deg. At larger SZAs (when absolute values are small), relative differences can be substantial. The agreement is generally better for data products that are not (or only slightly) sensitive to atmospheric ozone concentration. The scatter in the ratio of both instruments is somewhat larger during cloudy periods, which is due to the different sampling schemes of the two instruments. The GUV reports 1-min averages, whereas the SUV requires several minutes to scan between 290 and 400 nm. Radiation levels may change during this period. Differences in the cosine errors of the two instruments cause the diurnal variation in the ratio for UV-A on day 1 [Fig. 6(d)]. In contrast, there is little variation on the overcast day 3, when the radiation field was more isotropic.

A comparison based on data from 3 days is insufficient to quantify uncertainties of GUV data products related to instrument drift, variation in total ozone, or site-specific differences (e.g., variation in albedo). To quantify long-term behavior, we compared seven GUV data products with the respective SUV-100 data over 1-yr periods at all four sites. The associated statistics are presented in Table 3 and further explained in the following. The following seven data products were chosen: UV index[11]; DNA-damaging radiation[17]; generalized plant damage[19]; and the integrals 290 to 315, 290 to 320, 320 to 360, and 320 to 400 nm. Note that there are two data sets for the South Pole in Table 3 that are based on identical raw data. The second data set was calculated with cosine-corrected SUV data.[25] The statistics of the two data sets are very similar, indicating that most of the observed differences of GUV and SUV data products were not caused by the cosine error.

In the first evaluation step, GUV and SUV-100 data

Table 3 Statistics of comparison of GUV and SUV data products.

Data Product	Slope	R^2	Average SZA<80 deg	St. Dev. SZA<80 deg	SZA_{max} (deg)	Average SZA<SZA_{max}	St. Dev. SZA<SZA_{max}	E_{max}[a]	E_{min}/E_{max}
San Diego, GUV-511 S/N 9298, volume 12 (8/16/02 to 8/19/03)									
UV index	1.003	0.9980	1.010	0.040	82	1.008	0.042	10.5	0.010
DNA damage	1.035	0.9949	1.171	1.544	34	1.042	0.059	0.537	0.313
Plant damage	0.998	0.9973	0.989	0.130	72	1.012	0.060	8.50	0.013
UV-B (290 to 315 nm)	1.002	0.9967	1.010	0.073	75	1.015	0.056	191	0.018
UV-B (290 to 320 nm)	0.995	0.9976	1.002	0.043	78	1.004	0.041	349	0.020
320 to 360 nm	1.003	0.9972	1.012	0.034	93	1.011	0.033	2444	0.004
UV-A (320 to 400 nm)	1.001	0.9987	1.014	0.029	93	1.012	0.034	6216	0.003
South Pole, GUV-541 S/N 29239, volume 13 (1/17/03 to 1/20/04)									
UV index	1.003	0.9991	1.002	0.018	91	1.012	0.025	2.5	0.007
DNA damage	1.000	0.9969	1.009	0.039	81	1.007	0.042	0.076	0.185
Plant damage	1.004	0.9978	1.001	0.042	82	1.004	0.047	1.51	0.135
UV-B (290 to 315 nm)	1.019	0.9988	1.024	0.026	80	1.024	0.026	50	0.185
UV-B (290 to 320 nm)	1.001	0.9990	1.002	0.019	90	1.024	0.042	111	0.006
320 to 360 nm	1.000	0.9979	0.997	0.026	92	0.986	0.031	1316	0.004
UV-A (320 to 400 nm)	0.999	0.9973	0.997	0.029	92	0.985	0.031	3133	0.004
South Pole, GUV-541 S/N 29239, volume 13 (1/17/03 to 1/20/04), cosine corrected									
UV index	0.994	0.9990	0.992	0.017	90	1.004	0.027	2.7	0.007
DNA damage	0.999	0.9967	1.007	0.038	81	1.006	0.041	0.080	0.185
Plant damage	1.003	0.9977	1.001	0.042	80	1.001	0.042	1.60	0.150
E 290 to 315	1.009	0.9987	1.015	0.026	80	1.015	0.026	54	0.185
E 290 to 320	0.990	0.9990	0.992	0.018	90	1.017	0.046	119	0.006
E 320 to 360	0.987	0.9978	0.982	0.025	92	0.977	0.027	1426	0.004
UV-A (320 to 400 nm)	0.983	0.9973	0.978	0.027	92	0.974	0.026	3406	0.003
Palmer, GUV-511 S/N 29230, volume 12 (7/17/02 to 3/17/03)									
UV index	1.006	0.9993	1.015	0.029	81	1.014	0.031	7.4	0.020
DNA damage	0.996	0.9962	1.076	0.461	54	0.981	0.054	0.373	0.121
Plant damage	1.009	0.9983	0.983	0.245	61	1.022	0.041	5.88	0.058
UV-B (290 to 315 nm)	1.011	0.9979	1.042	0.079	66	1.025	0.045	142	0.088
UV-B (290 to 320 nm)	1.005	0.9988	1.016	0.037	79	1.017	0.035	282	0.025
320 to 360 nm	0.998	0.9990	0.995	0.022	93	0.996	0.030	2363	0.001
UV-A (320 to 400 nm)	0.997	0.9993	0.994	0.021	93	0.992	0.029	5637	0.001
McMurdo, GUV-511 S/N 29234, volume 12 (3/6/02 to 1/13/03)									
UV index	0.965	0.9986	0.944	0.042	78	0.951	0.038	4.7	0.071
DNA damage	0.890	0.9762	1.463	1.172	—	—	—	0.145	0.729
Plant damage	1.005	0.9983	0.882	0.353	73	1.011	0.055	2.89	0.042
UV-B (290 to 315 nm)	1.019	0.9971	1.001	0.158	75	1.042	0.056	93	0.042
UV-B (290 to 320 nm)	0.995	0.9985	0.981	0.057	76	0.997	0.036	201	0.071
320 to 360 nm	0.977	0.9985	0.969	0.026	93	0.957	0.027	1991	0.003
UV-A (320 to 400 nm)	0.977	0.9979	0.972	0.032	93	0.961	0.031	4758	0.003
McMurdo, GUV-511 S/N 29234, volume 13 (1/29/03 to 2/1/04)									
UV index	0.988	0.9991	0.976	0.031	82	0.971	0.034	5.6	0.038
DNA damage	0.920	0.9842	1.041	0.425	55	0.931	0.041	0.223	0.430
Plant damage	1.022	0.9990	1.013	0.083	77	1.033	0.043	4.04	0.025
UV-B (290 to 315 nm)	1.035	0.9980	1.064	0.058	71	1.048	0.043	108	0.150
UV-B (290 to 320 nm)	1.015	0.9988	1.020	0.034	81	1.018	0.036	216	0.038
320 to 360 nm	0.996	0.9985	0.989	0.028	93	0.980	0.029	1939	0.002
UV-A (320 to 400 nm)	0.995	0.9983	0.991	0.030	93	0.981	0.031	4421	0.003

[a]Units of E_{max} is microwatts per square centimeter except for UV index, which has no unit.

products were regressed against each other using measurements from all SZAs. With the exception of DNA-damaging irradiance, slope values of the regression ranged between 0.977 and 1.035, and the associated regression coefficients R^2 varied between 0.976 and 0.999. For DNA-damaging irradiance, slope values were as low as 0.89, and R^2 was as low as 0.976. In a second step, ratios of GUV and SUV data were calculated for the seven data products using only measurements when the SZA was smaller than 80 deg. The average of these ratios varied between 0.944 and 1.064, with the exceptions of larger discrepancies for DNA-damaging irradiance and plant-damaging irradiance

from McMurdo data for volume 13. The standard deviations of the ratios ranged between 0.018 and 0.097, except for DNA- and plant-damaging irradiances, where values were higher.

Slope, R^2, average, and standard deviation values indicate that the conversion algorithm works reasonably well for all but DNA-damaging irradiance. On average, systematic differences are smaller than 7% (worst case) and the scatter between the GUV and SUV-100 data sets is of the order of ± 2 to 10% at the one σ level. Results for DNA-damaging irradiance are considerably worse, with the exception of results from the South Pole. The South Pole is the only site where a GUV-541 radiometer is installed, which has a channel at 313 nm rather than PAR. The effect of the added channel is discussed in Sec. 6.

Large relative errors may be inconsequential if they occur at large SZAs or low absolute values. We therefore calculated maximum SZAs (SZA_{max}) and minimum irradiance values (E_{min}) for which data can trusted. To calculate SZA_{max}, we first sorted all data into 1-deg-wide SZA bins. The value of SZA_{max} is based on the condition that at least 90% of GUV and SUV-100 measurements agree with each other to within $\pm 15\%$ for all bins with SZA less than SZA_{max}. The minimum irradiance E_{min} is similarly defined: at least 90% of GUV and SUV-100 measurements must agree with each other to within $\pm 15\%$ when SUV-100 measurements are larger than E_{min}. Table 3 specifies the ratio E_{min}/E_{max}, where E_{max} is defined as the maximum value observed by the SUV-100 for a given site, year, and data product. For example, if E_{min}/E_{max} is 0.01, values can be trusted if they are larger than 1% of the annual maximum.

For the UV index, SZA_{max} is typically 80 deg (90 deg for South Pole). For the 320- to 360- and 320- to 400-nm integrals, SZA_{max} is larger than 90 deg for all sites. Maximum SZAs for all but DNA-damaging irradiance vary between 61 and 80 deg. The value for SZA_{max} for DNA-damaging irradiance is smaller than 50 deg (81 deg for South Pole). Values of E_{min}/E_{max} range between 0.001 (for UV-A) and 0.185 for all but DNA-damaging irradiance, where E_{min} may be as large as 0.729. For the majority of data products and sites, E_{min}/E_{max} is smaller than 0.1.

In the last evaluation step, data were filtered for SZAs less than SZA_{max} and the calculation of average and standard deviation of the GUV/SUV ratio was repeated. Average ratios of this subset varied between 0.931 and 1.048 for all sites and data products (including DNA damage), and the associated standard deviations ranged between 0.025 and 0.060. There is evidence that most variation is caused by the different GUV and SUV sampling schemes rather than the conversion procedure.

4.2 *Total Column Ozone*

Total ozone column is calculated from GUV measurements with look-up tables, which relate total column ozone to SZA and the ratio of GUV measurements at 305 and 340 nm. The retrieval method is similar to the method described by Stamnes et al.[26] Look-up tables were calculated with the radiative transfer model UVSPEC/libRadtran, and resulting model spectra were weighted with the GUV response functions at 305 and 340 nm. Separate look-up tables were calculated for each site, taking into account site-specific conditions such as altitude, albedo, ozone profile, etc.

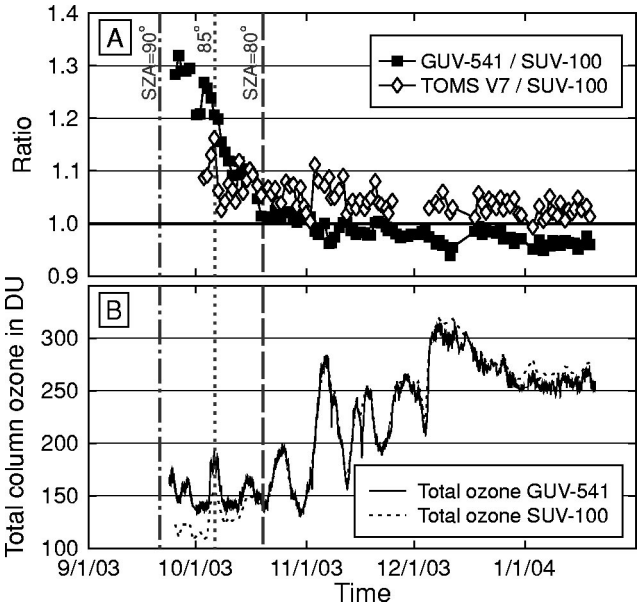

Fig. 7 Comparison of total column ozone measured at the South Pole by GUV-541 S/N 29239, SUV-100, and NASA's TOMS instrument on board the earth probe satellite in the austral spring of 2003.

Figure 7 presents a comparison of total ozone measured at the South Pole during the austral spring of 2003 by GUV-541 and SUV-100 instruments as well as the National Aeronautics and Space Administration's (NASA's) total ozone mapping spectrometer (TOMS) on board the earth probe satellite. TOMS data are from the TOMS Version 7 data set. SUV-100 ozone values were derived with an algorithm that has recently been proposed by Bernhard et al.[27] This algorithm takes the variations of the ozone profile into account and is therefore more accurate at large SZAs than the method implemented for GUV data. For SZAs smaller than 80 deg, GUV ozone values are $2 \pm 2\%$ smaller than SUV values. For larger SZAs, GUV data significantly overestimates the actual ozone column, which may partly be due to ozone profile effects. In comparison, TOMS observations exceed SUV-100 measurements by $4.5 \pm 3.0\%$, but there is no obvious change in the ratio of the two data sets when SZAs become larger than 80 deg. It has been noted elsewhere that TOMS Version 7 data overestimate the actual ozone column by 5 to 10% at high southern latitudes.[28,29] Our preliminary comparison of the recently released Version 8 TOMS data set with SUV-100 data indicates that this bias has mostly disappeared.

GUV total ozone data have been compared at all sites with TOMS Version 7 ozone observations (Table 4). On average, GUV and TOMS data agree to within $\pm 5\%$. The standard deviation of the ratio of both data sets is typically 5%, and GUV measurements can be trusted up to SZAs of 80 to 85 deg.

5 Web Site Implementation

GUVs at network sites are controlled by individual workstations where the raw data is also stored. Raw data are remotely harvested from the logging computers, and all

Table 4 Comparison of GUV and NASA earth probe TOMS total ozone values.

Site	Instrument	Comparison Period	SZA Range (deg)	Ratio GUV/TOMS			SZA_{max} (deg)
				Average	Median	St. Dev.	
San Diego	GUV-511 S/N 9298	08/16/02 to 08/18/03	18 to 63	0.96	0.96	0.03	85
South Pole	GUV-541 S/N 29239	10/18/03 to 01/19/04	67 to 81	0.95	0.95	0.05	80
Palmer	GUV-511 S/N 29230	08/12/02 to 03/17/03	41 to 80	1.01	1.02	0.05	82
McMurdo	GUV-511 S/N 29234	01/30/03 to 02/01/04	55 to 83	1.03	1.04	0.05	82

Only GUV data measured coincidently with the TOMS satellite overpass were used.
SZA_{max} is the maximum SZA up to which GUV total ozone values can be trusted.

data products listed in Table 2 are calculated and presented at the Webpage www.biospherical.com/nsf/login/update.asp as soon as available. Depending on the location and availability of Internet connectivity to Antarctic sites, datasets are updated either every minute, every hour, or daily. The Webpage includes graphs of the UV index, PAR, and total ozone. Other data products can be selected by means of an easy-to-use Web interface. Data in ASCII format is also available for download.

6 Discussion and Conclusions

Several moderate-bandwidth, multichannel GUV filter radiometers were characterized for their spectral response and calibrated against SUV spectroradiometers and standard lamps. Response functions were measured over 3 to 3.5 orders of magnitude (Fig. 2) using a new spectral characterization apparatus (Sec. 2). Results from different GUVs suggest that the response functions for the same nominal wavelength can differ by as much as 1.0 nm due to differences in individual transmission characteristics of the interference filters used.

When measured response functions were used in GUV calibrations, GUV and SUV-150B measurements agreed to within $\pm 5\%$ for SZAs smaller than 85 deg (Fig. 3). To simulate the effect of imprecisely known response functions, we shifted the functions of GUV S/N 9298 by 0.5 nm and repeated calibration and comparison. When the shifted functions were used, the ratio of measurements of the two instruments showed a large SZA dependence at 305 nm, with a maximum deviation of 14% at SZA=75 deg [Fig. 4(a)]. Deviations for the other channels were smaller than 5% [Fig. 4(b)], indicating that accurate knowledge of the instrument's response functions is less critical at UV-A wavelengths. When the correct functions were used, solar and lamp-based calibration factors agreed to within $\pm 3\%$ (Fig. 5), suggesting that lamp-based GUV calibrations are feasible even for the 305-nm channel. This is a significant improvement compared to previously reported results.[4] On the other hand, solar data from 305 nm may be incorrect by more than 10% if the calibration factor of this channel is established from a lamp measurement and the response function used for the calculation has a wavelength error of 0.5 nm. As response functions may vary by several tenths of 1 nm from instrument to instrument, spectral characterization of each instrument appears to be necessary to gain results with sufficient accuracy. However, if GUVs are calibrated against an accurate spectroradiometer, it may be sufficient to use a generic response function and shift it until the ratio GUV/spectroradiometer becomes independent of SZA. This approach has been successfully implemented for GUVs S/N 29230 and 29234 (Sec. 4). Differences between actual and generic functions may exist for some instruments that cannot be characterized by a shift of the center wavelength alone. For example, Fig. 2 indicates that the difference between the 305-nm filters of GUVs S/N 9298 and 29236 is substantial. To avoid calibration errors related to inaccurately known response functions, and to gain the most accurate solar data, we believe that a thorough characterization of all channels is advisable.

In the second evaluation step, various UV data products were calculated from calibrated GUV data using the inversion algorithm suggested by Dahlback.[3] Results of the algorithm were validated against SUV-100 measurements at San Diego, the South Pole, McMurdo, and Palmer Stations. For UV-A irradiance, GUV and SUV data agreed to within a few percent up to a SZA of 90 deg (Table 3), showing that UV-A irradiance can be accurately calculated even at twilight from three GUV channels (i.e., 320, 340, and 380 nm). A similar good agreement between GUV and SUV measurements can be achieved for the UV index and the 290- to 320-nm integral if solar measurements are restricted to SZAs smaller than 78 deg. At greater SZAs, irradiance levels are typically less than 5% of their annual maximum. Larger relative differences were calculated for the integral 290 to 315 nm and plant-damaging irradiance. While GUV and SUV measurements of these data products still agreed on average to within $\pm 5\%$, the scatter in data of the two instruments is clearly increased for SZAs greater than 70 deg. For example, the standard deviation of the ratio GUV/SUV for ''plant damage'' is 13% at San Diego when data up to a SZA of 80 deg are used. On the other hand, if solar measurements are restricted to SZAs smaller than 72 deg, the agreement is similar to that for UV-A irradiance. At SZA=72 deg, irradiance levels are smaller than 1.5% of the annual maximum, suggesting that the increased variation for larger SZAs is inconsequential for most applications.

DNA-damaging radiation is the only GUV-511 data product where the results are clearly not satisfactory, with the exception of results from the South Pole. The South Pole is the only site where a GUV-541 radiometer, which has an additional UV channel at 313 nm, is installed. Using the GUV-541, DNA-damaging radiation is calculated from measurements at four channels (305, 313, 320, and 340 nm) rather than three channels, as is the case for the GUV-511 at the other sites. It appears that three channels are not sufficient to characterize the SZA and ozone dependence of data products that are heavily weighted toward short UV-B

wavelengths, such as DNA-damaging irradiance. South Pole data demonstrate that four channels are sufficient: the average ratio GUV/SUV is 1.009 for SZAs smaller than 80 deg and the corresponding standard deviation is 0.039. Note that GUV-541 instruments were not installed at other sites because of the missing PAR channel. PAR is operationally more important at these other locations than the increased accuracy of UV data products.

Total column ozone values calculated from GUV measurements with look-up tables agree with TOMS Version 7 ozone observations on average to within ±5% (Table 4). GUV ozone values can typically be trusted up to SZAs of 80 to 85 deg (Fig. 7).

It has been shown that high-resolution spectra can be reconstructed from multifilter radiometers by means of radiative transfer modeling.[5,30] These spectra can then be weighted with any action spectrum to calculate UV data products. This method is an alternative to the inversion method evaluated in this paper. The uncertainties of both methods have yet to be compared. For the objectives of the NSF/OPP network, we decided to use the inversion method since it does not require radiative transfer modeling of every spectrum and is therefore easier to implement in a real-time data processing environment.

In summary, data from accurately characterized and calibrated, multichannel filter radiometers can provide reasonably accurate measurements of biologically relevant UV levels and total column ozone. In comparison with spectroradiometers, they are easier to operate, which may provide an advantage in supplying calibrated data in real time. Furthermore, filter instruments are easier to deploy and maintain due to their simpler design, and offer data at higher sampling rates. Although drifts in sensitivity over time (e.g., 4% per annum) have been reported,[9] filter radiometers usually have a better short-term stability than spectroradiometers. This makes them useful for quality control of spectroradiometric measurements.

Acknowledgments

The NSF/OPP UV Monitoring Network is operated and maintained by Biospherical Instruments Inc. under contracts from the NSF Office of Polar Programs (Dr. Polly Penhale) via Raytheon Polar Services. The design and construction of the spectral test apparatus was overseen by David Goebel. We thank Patrick Disterhoft from the National Oceanic and Atmospheric Administration (NOAA's) Central UV Calibration Facility for providing the xenon lamp used in the spectral test apparatus. The Website implementation was programmed by Vi Quang. We thank John Morrow for his critical comments concerning the manuscript.

References

1. C. R. Booth, T. B. Lucas, J. H. Morrow, C. S. Weiler, and P. A. Penhale, ''The United States National Science Foundation's polar network for monitoring ultraviolet radiation,'' *Antarc. Res. Ser.* **62**, 17–37 (1994).
2. G. Bernhard, C. R. Booth, J. C. Ehramjian, and V. V. Quang, *NSF Polar Programs UV Spectroradiometer Network 2000–2001 Operations Report*, Biospherical Instruments Inc., San Diego, CA (2003).
3. A. Dahlback, ''Measurements of biologically effective UV doses, total ozone abundances, and cloud effects with multichannel, moderate bandwidth filter instruments,'' *Appl. Opt.* **35**(33), 6514–6521 (1996).
4. C. R. Booth, T. Mestechkina, and J. H. Morrow, ''Errors in the reporting of solar spectral irradiance using moderate bandwidth radiometers: an experimental investigation,'' in *Ocean Optics XII*, *Proc. SPIE* **2258**, 654–663 (1994).
5. C. R. Booth, ''Synthetic UV spectroradiometry,'' in *IRS'96 Current Problems in Atmospheric Radiation*, W. L. Smith and K. Stamnes, Eds., pp. 849–852, A. Deepak Pub., Hampton, VA (1997).
6. H. A. Fuenzalida, ''Global ultraviolet spectra derived directly from observations with multichannel radiometers,'' *Appl. Opt.* **37**(33), 7912–7919 (1998).
7. T. M. Thorseth and B. Kjeldstad, ''All-weather ultraviolet solar spectra retrieved at a 0.5 Hz sampling rate,'' *Appl. Opt.* **38**(30), 6247–6252 (1999).
8. T. M. Thorseth, B. Kjeldstad, and B. Johnsen, ''Comparison of solar UV measurements performed with spectroradiometer and moderate bandwidth multichannel radiometer for different cloud conditions,'' *J. Geophys. Res.* **105**(D4), 4809–4820 (2000).
9. B. Johnson, O. Mikkelborg, M. Hannevik, L. T. Nilsen, G. Saxebol, and K. G. Blaasaas, *The Norwegian UV-monitoring program. Period 1995/96 to 2001*, Strålevern Rapport 2002:4, Norwegian Radiation Protection Authority, Østerås, Norway (2002).
10. A. F. McKinlay and B. L. Diffey, ''A reference action spectrum for ultraviolet induced erythema in human skin,'' *CIE Res. Note* **6**(1), 17–22 (1987).
11. World Meteorology Organisation (WMO), *Report of the WMO-WHO Meeting of Experts on Standardization of UV Indices and Their Dissemination to the Public*, Global Atmospheric Watch Report No. 127, WMO, Geneva, Switzerland (1998).
12. K. Lantz, P. Disterhoft, E. A. Early, J. DeLuisi, A. Thompson, J. Berndt, L. Harrison, P. Kiedron, J. Ehramjian, G. Bernhard, L. Cabasug, J. Robertson, W. Mou, T. Taylor, J. Slusser, D. Bigelow, B. Durham, G. Janson, D. Hayes, M. Beaubien, and A. Beaubien, ''The 1997 North American interagency intercomparison of ultraviolet spectroradiometers including narrowband filter radiometers,'' *J. Res. Natl. Inst. Stand. Technol.* **107**, 19–62 (2002).
13. B. Mayer, G. Seckmeyer, and A. Kylling, ''Systematic longterm comparison of spectral UV measurements and UVSPEC modeling results,'' *J. Geophys. Res.* **102**(D7), 8755–8768 (1997); the radiative transfer model UVSPEC/libRadtran is also available at www.libradtran.org.
14. W. D. Komhyr and L. Machta, ''The relative response of erythema,'' in *The Perturbed Troposphere of 1990 and 2020*, Vol. IV, CIAP, Dept. of Transportation, Washington, DC (1973).
15. B. L. Diffey, ''A comparison of dosimeters used for solar ultraviolet radiometry,'' *Photochem. Photobiol.* **46**, 55–60 (1987).
16. A. Anders, H.-J. Altheide, M. Knaelmann, and H. Tronnier, ''Action spectrum for erythema in humans investigated with dye lasers,'' *Photochem. Photobiol.* **61**(2), 200–205 (1995).
17. R. B. Setlow, ''The wavelengths in sunlight effective in producing skin cancer: a theoretical analysis,'' *Proc. Natl. Acad. Sci. U.S.A.* **71**(9), 3363–3366 (1974).
18. F. R. Gruijl, H. J. C. M. Sterenborg, P. D. Forbes, R. E. Davies, C. Cole, G. Kelfkens, H. van Weelden, H. Slaper, and J. C. van der Leun, ''Wavelength dependence of skin cancer induction by ultraviolet irradiation of albino hairless mice,'' *Cancer Res.* **53**, 53–60 (1993).
19. M. M. Caldwell, ''Solar UV irradiation and the growth and development of higher plants,'' Chap. 4 in *Photophysiology*, Vol. 6, A. C. Giese, Ed., Academic Press, New York, pp. 131–177 (1971).
20. S. D. Flint and M. M. Caldwell, ''A biological spectral weighting function for ozone depletion research with higher plants,'' *Physiol. Plant.* **117**, 137–144 (2003).
21. J. H. Hunter, J. H. Taylor, and H. G. Moser, ''The effect of ultraviolet irradiation on eggs and larvae of the northern anchovy, *Engraulis mordax*, and the pacific mackerel, *Scomber japonicus*, during the embryonic stage,'' *Photochem. Photobiol.* **29**, 325–338 (1979).
22. N. P. Boucher and B. B. Prezelin, ''An in situ biological weighting function for UV inhibition of phytoplankton carbon fixation in the Southern Ocean,'' *Mar. Ecol.: Prog. Ser.* **144**, 223–236 (1996).
23. J. J. Cullen, P. J. Neale, and M. P. Lesser, ''Biological weighting function for the inhibition of phytoplankton photosynthesis by ultraviolet radiation,'' *Science* **258**, 646–649 (1992).
24. P. J. Neale and D. J. Kieber, ''Assessing biological and chemical effects of UV in the marine environment: spectral weighting functions,'' in *Issues in Environmental Science and Technology No. 14*, R. E. Hester and R. M. Harrison, Eds., Royal Society of Chemistry, Cambridge, UK (2000).
25. G. Bernhard, C. R. Booth, and J. C. Ehramjian, ''Version 2 data of the National Science Foundation's Ultraviolet Radiation Monitoring Network: South Pole,'' *J. Geophys. Res.* (in press); see also www.biospherical.com/nsf/Version2/Version2.asp.
26. K. Stamnes, J. Slusser, and M. Bowen, ''Derivation of total ozone abundance and cloud effects from spectral irradiance measurements,'' *Appl. Opt.* **30**(30), 4418–4426 (1991).
27. G. Bernhard, C. R. Booth, and R. McPeters, ''Calculation of total column ozone from global UV spectra at high latitudes,'' *J. Geophys. Res.* **108**(D17), 4532 (2003).

28. G. E. Bodeker, J. C. Scott, K. Kreher, and R. L. McKenzie, ''Global ozone trends in potential vorticity coordinates using TOMS and GOME intercompared against the Dobson network: 1978–1998,'' *J. Geophys. Res.* **106**(D19), 23029–23042 (2001).
29. G. Bernhard, C. R. Booth, and J. C. Ehramjian, ''Comparison of measured and modeled spectral ultraviolet irradiance at Antarctic stations used to determine biases in total ozone data from various sources,'' in *Ultraviolet Ground- and Space-based Measurements, Models, and Effects*, J. R. Slusser, J. R. Herman, and W. Gao, Eds., *Proc. SPIE* **4482**, 115–126 (2002).
30. Q. Min and L. Harrison, ''Synthetic spectra for terrestrial ultraviolet measurements,'' *J. Geophys. Res.* **103**(D14), 17033–17039 (1998).

Biographies and photographs of authors not available.